2022

Influence of Growth Parameters on the Synthesis of MoS2 Films

Victor Okonkwo
University of Central Florida

INFLUENCE OF GROWTH PARAMETERS ON THE SYNTHESIS OF MOS_2 FILMS

by

VICTOR CHUWKWUDUBEM OKONKWO

A thesis submitted in partial fulfillment of the requirements
for the Honors in the Major Program in Materials Science and Engineering
in the College of Engineering and Computer Science
and in the Burnett Honors College
at the University of Central Florida
Orlando, Florida

Summer Term, 2022

Thesis Chair: Tania Roy, Ph.D.

ABSTRACT

Information processing is crucial in modern society, placing a great emphasis on the performance of optoelectronic devices to match ever increasing processing and memory needs. Within these devices, MoS_2 has demonstrated great potential as transistors due to its enhanced electrostatic control. As increased layer thickness of quality MoS_2 films have been shown to boost the performance of its transistors, growth parameters for the synthesis of ideally uniform and large area multilayered films via chemical vapor deposition were investigated. By increasing the flow pressure in the system and the growth time, increasing levels of thickness and nucleation density was shown for MoS_2 growth. Although the scale of the growth was non-uniform in nature, films containing large areas of thicker MoS_2 was achieved. The thickness of the films was confirmed by Raman and photoluminescence measurements by confirming their values with exfoliated MoS_2 measurements.

TABLE OF CONTENTS

LIST OF FIGURES

INTRODUCTION

Today, the amount of available information for processing is ever-increasing. Subsequently, current computational technology is experiencing greater difficulties in attaining and retaining the expanding storage of information efficiently, while trying to offset increasing demand in higher performance. Originally computing devices relied on von Neumann architecture for processing and retaining information. In this architecture, a central processing unit (CPU) is responsible for acquiring data and executing commands, while a separate memory unit stores instructions and data. [1] However, due to 2 classes of memory (programming and data) sharing a single bus to the CPU, only one type may be transferred at a time, severely limiting the rate of data transfer. [2] Referred to as the von Neumann bottleneck, the rate of data transfer is much lower than the speed of the CPU, producing low effective processing speeds and overall energy efficiency. Incorporation of evolving transistors in the architecture has succeeded in improving the hardware by increasing the processing speed of the CPU, however fabrication limits have halted the progress as transistors have been downscaled to its physical limits of 10 nm. [3] Even then, the lag between processing and memory units persists as the gap in the improvement of the CPU speed and memory storage size continues to outpace improvements in data transfer. To circumvent this issue, a neuromorphic system of devices functioning like the human brain was proposed by Carver Mead. [4] Similar to the neural network in the brain, devices would be able to process and learn information simultaneously. To achieve this, early neuromorphic circuits adopted the Hodgkin-Huxley model, resistor-capacitor circuits with a battery, to model the action

potential in neurons and integrate processing and learning. [5] However it faced setbacks due to requiring multiple devices to enable learning and memory within the area limitations of a single chip.

To improve integration in neuromorphic devices, photoelectric memristors were implemented, combining both detection and memory units. The resistance of the memristor changes accordingly to light stimuli and manages to retain its conductance upon removal of said stimuli, displaying nonvolatile memory. [6] Usage of bulk materials such as transition metal oxides was first implemented, but later found to have many disadvantages mainly due to the strong influence their dangling bonds and uncontrollable surface defects have on the device response. [7] Problems such as random filament formation causing device-to-device variation, non-linear conductance change, and inadequate conductance states manifest in these devices [8]. In comparison, 2D layer materials have dangling-bond-free surfaces and controllable defects due to their saturated covalently bonded lattice permitting device integration without regard to crystal lattice matching. [9] Furthermore, the thinner atomic thickness of 2D materials permits a higher memory phase due to higher sensitivity to charges stored in the gate channel. The transfer processes involved also allow easy transfer of 2D materials to any potential substrate, increasing potential combinations and structures. Finally, the bandgap of 2D materials, specifically transition metal dichalcogenides, enable high photoresponsivity to light in the visible spectrum, applicable to many fields of information processing.

Of the transition metal dichalcogenides, the functionality of MoS_2 field effect transistors will be observed. MoS_2 has been proven to be a great transistor due to its enhanced electrostatic control of the gate throughout its channel, offering high carrier mobilities (200 $cm^2\ V^{-1}\ s^{-1}$) and

on/off ratios (1×10^8). [10] Although monolayer MoS_2 growth has seen success in research, controllable growth of multilayered MoS_2 films have proven much more difficult. The alternative option, exfoliation bulk MoS_2 films, is handicapped as it has no control over the size and number of layers produced. [11] In the observed exfoliated multilayered films, the transistor is observed to have greater carrier mobility and higher on-state current.

Previous literature has shown considerable success in producing multilayer growth via chemical vapor deposition (CVD) with MoO_3 and S_2 precursors. [11-15] However, the main issue with these precursors is that their reaction may lead to the formation of byproducts like MoO_2 during the synthesis, introducing impurities in the film that hinder device performance. [16] As a result, the use of single precursor MoS_2 will be investigated. In this paper, the results of CVD growth from the variation in flow pressure and growth time are reported and their impact on layer thickness and uniformity of MoS_2 films are observed. The film thickness of the samples is measured and characterized by Raman spectroscopy and photoluminescence (PL) for further confirmation.

EXPERIMENTAL SECTION

CVD Synthesis for MoS_2 Growth

The CVD schematic is shown in Figure 1. For large area and quality synthesis of MoS_2, chemical vapor deposition was carried out in the MTI OTF-1200X two zone furnace. For each run, 500 mg of MoS_2 precursor (Sigma-Aldrich 99.999%) was weighted and added to a quartz boat. The boat was placed in a 1-inch quartz tube, centered in the first zone. 285 nm SiO_2 on Si was used as substrate and cut as 1.2 cm^2 samples. 5 samples were placed downstream of the precursor boat, starting at 1 cm from the edge and lining up to 7 cm away. Prior to placement, the samples were treated with ultrasonication in acetone for 10 minutes, then rinsed with acetone and isopropyl alcohol afterwards. They were then blow-dried with N_2 gas. After substrate placement, the system was sealed and pumped down in vacuum down to a pressure below 25 mT. From there the system is heated up to a 950°C in 95 minutes with Argon carrier gas flowing through the tube.

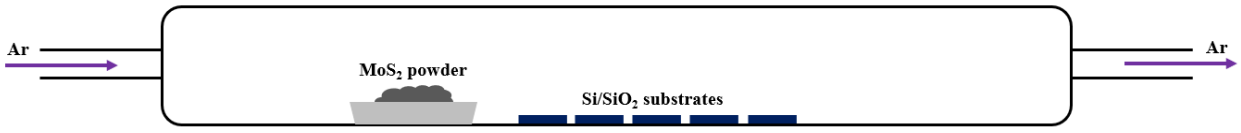

Figure 1: Diagram of CVD setup

The temperature was held for a growth time between 25-60 minutes at constant carrier gas flow rate and tube pressure of 100 and 1.75 Torr respectively. Afterwards, the system was

left to cool down gradually to 350°C and then rapidly cooled by opening furnace's lid. The trend in growth was observed for the varied growth times. The flow rate of carrier gas and subsequently the pressure of the tube were then varied between 1-3 Torr and the effects on growth were also studied.

MoS_2 Characterization

The Renishaw RM 1000B Micro-Raman Spectrometer was used to perform Raman spectroscopy at an excitation of 514 nm. Photoluminescence analysis was performed with the WITec Alpha300 at an excitation of 532 nm and 10s integration time.

RESULTS AND DISCUSSION

Optical Microscopy

Fig 2(a)-(c) depicts optical images for three separate MoS_2 films grown simultaneously during CVD synthesis at different distances from the quartz boat. During the synthesis, the furnace was subjected to a growth temperature of 950°C, flow pressure of 1.75 Torr, growth times of 30 minutes, and 500 mg MoS_2 precursor. Layer thickness and morphology of MoS_2 is greatly affected by the distance of the substrate from the precursor. At 3 cm away, triangular MoS_2 flakes of 3+ layers observed with a large portion of background growth containing bilayer thickness as shown in Fig. 2(a). At 5 cm away, the thicker triangular flakes disappear and are replaced by smaller notched bilayer flakes. Underneath, continuous MoS_2 monolayer is found.

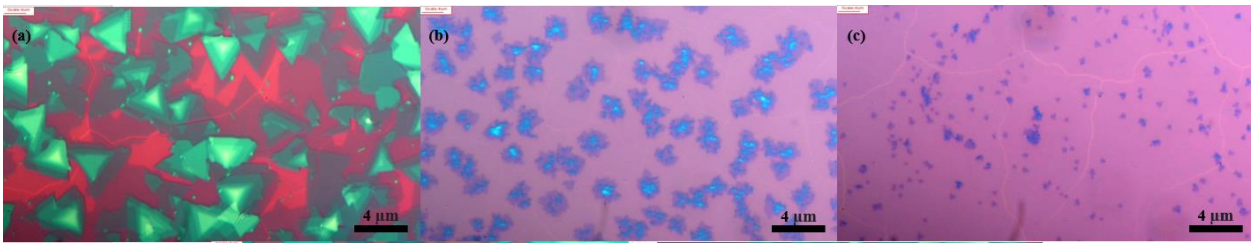

Figure 2: Optical images of MoS_2 films with varying downstream distances from the MoS_2 precursor at (a) 3 cm (b) 5 cm and (c) 7 cm

Shifting to 7 cm away, further downsizing of bilayer flakes is observed, with majority of the film constituting of MoS_2 monolayer. Figure 2 demonstrates that growth between 3 and 7 cm downstream of the precursor is sufficient for growth and guarantees film coverage due to being

within the range of the gaseous MoS_2 boundary layer, permitting deposition. [17] Substrates closer than 3 cm from the precursor are unable to achieve any growth due to the temperature being well above the deposition temperature of 450 ºC. Due to limitations via diffusion, increasing the distance from the precursor reduces the amount of available MoS_2 for deposition. According to classic crystal growth theory, gaseous MoS_2 deposit and adsorb into theSiO_2 substrate forming thermodynamically stable triangle nuclei during the seeding process. [18] The MoS_2 nuclei then requires continual precipitation of MoS to support the formation of the observed triangular MoS_2 flakes as growth occurs from the edge of the nuclei and expands laterally. Subsequently, lower supply of MoS_2 deposition affects nuclei expansion and results in smaller flake sizes. This explains the decrease in bilayer flake size with increasing distance from the precursor. The formation of continuous monolayer film is possible due to the self-limiting mechanism of MoS_2 growth where nucleation of each layer must occur before growth of the next layer [19]

Fig. 3(a)-(f) depicts optical images of MoS_2 films grown at varying growth times between 25 and 60 minutes. While growth time varied, consistent parameters of 1.75 Torr flow pressure, 950°C growth temperature, and 500 mg MoS_2 precursor were maintained. The samples shown in Figure 3 were all approximately 3-4 cm downstream of the precursor, at the optimal distance for multilayer growth as previously discussed. Between 25-35 minutes, the edge length of the multilayered flakes increases from 10 μm at 25 minutes, to 14 μm at 35 minutes. Past 35 minutes however, the positively correlated relationship between growth time and flake size disappears as smaller flake sizes become more common at 50-60 minutes as shown in Fig. 3(e)(f). The presence of multilayered flakes increases substantially with increasing growth time as substrates

subjected to 60 minutes have greater flake density than growth at 25 minutes. Regardless of growth time, the morphology of the multilayer flakes maintained their triangular shape. The observed trend in nucleation density and growth time results from an increase in available thermal energy, providing the means to overcome the adsorption energy barrier for MoS_2 on Si substrate. [20] Subsequently, greater nucleation centers form and give rise to higher flake density.

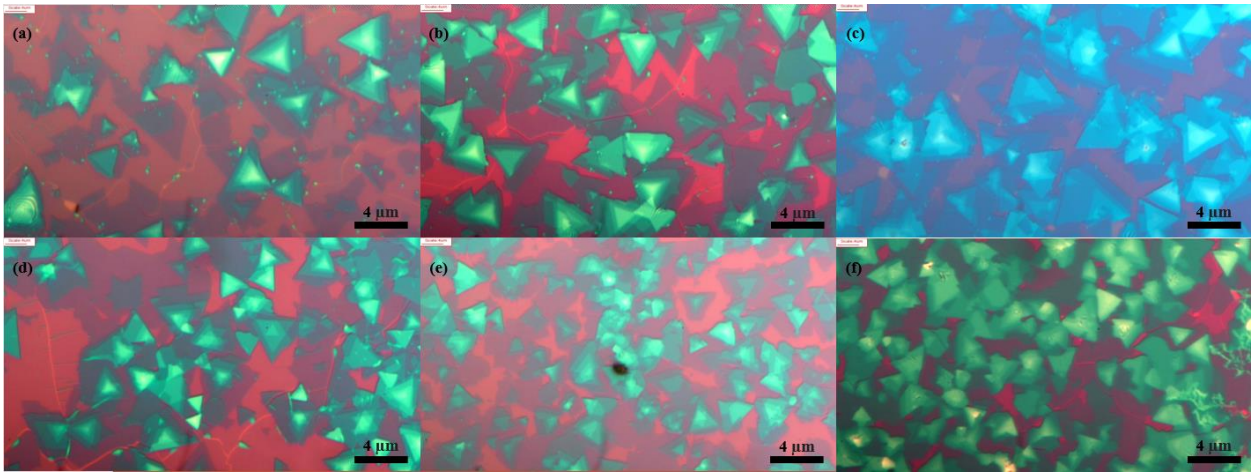

Figure 3: Optical images of MoS_2 films grown at varying growth times for (a) 25 minutes (b) 30 minutes (c) 35 minutes (d) 40 minutes (e) 50 minutes and (f) 60 minutes

However, increasing growth time substantially proved disadvantageous in that the number of impurities and surface defects increased as well. Samples grown for longer than 35 minutes displayed large areas of surface defects, limiting the coverage of the film. Figure 4 illustrates the portion of film affected by the surface defects. The depicted film is the same sample from Fig. 3(f) with smaller zoom. These defects may arise from chemisorption of oxygen in the substrate, disrupting the lattice. [21] At higher growth time, the system has longer susceptibility to oxygen leaks from the external environment which would provide the source for

the chemisorption. Considered, growth times around 30-35 minutes may be more ideal to avoid these defects.

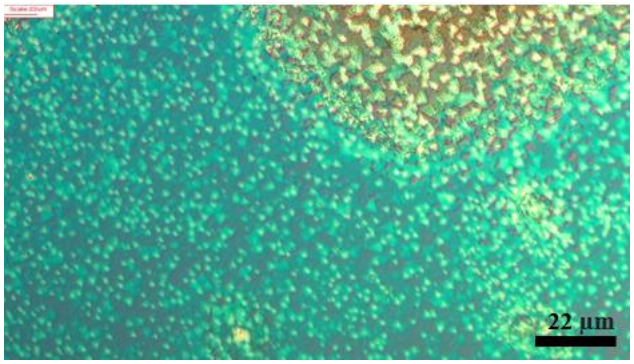

Figure 4: Optical image of MoS_2 film grown for 60 minutes depicting the surface defects plaguing the film

Figure 5(a)-(e) displays the optical images of MoS_2 films grown at varying flow pressures between 1-3 torr. The growth temperature and precursor amount were kept the same as in prior syntheses. A consistent growth time of 30 minutes was performed at each flow pressure. At 1 torr the film is seen to primarily be continuous monolayer with nanoparticles resulting from the growth mechanism of MoS_2, as shown in Fig. 5(a). Growth at 1.5 Torr demonstrates continuous monolayer as well, with larger bilayer flakes. Increasing flow pressure past 1.5 Torr shows a general trend of larger flake sizes and density, with growth at flow pressures of 2.4 and 3 Torr demonstrate higher multilayer flake density and flakes sizes up to 16 μm. This trend may be explained by a mass transport-limited regime where higher flow pressures induce greater diffusion of precursor, resulting in higher nucleation rate and density. [22] With more available precursor, greater adsorption at the edges of the nucleation center is possible resulting in lateral expansion and greater flake sizes at higher pressures.

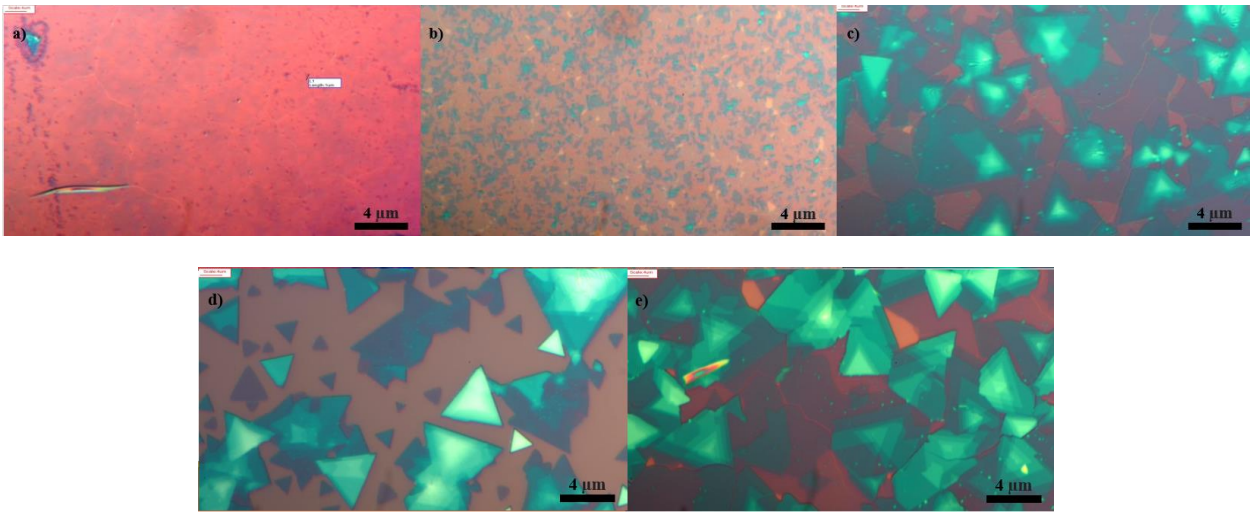

Figure 5: Optical images of MoS_2 films grown at various flow pressures for (a) 1.00 Torr (b) 1.5 Torr (c) 2.00 Torr (d) 2.4 Torr and (e) 3.00 Torr

MoS_2 Characterization

The Raman and PL spectra of select few samples were measured and analyze to confirm observations made from optical Microscopy. Figure 6 depicts the Raman and PL spectra for an MoS_2 film grown at 1.5 torr, akin to Figure 5(b). E^1_{2g} and A_{1g} are two signature peaks in the spectra for MoS_2, representing the in-plane and out-of-plane vibrations of the Mo-S bond. The difference in the frequencies between the two peaks is directly proportional to the number of layers of MoS_2; increase in the frequency difference is correlated with thicker and additional layers. [13] Layer thickness can be determined by comparison of frequency differences to exfoliated MoS_2. [22] PL analysis measures the intensity of the characteristic peak for the A

exciton of MoS_2. The intensity and excitation energy of the peak decreases with increasing layer thickness. [23] The sample shown in Figure 6(a)-(c) measured a peak difference of 19.16 cm^{-1} and exciton energy of 1.88 eV. These values agree match those of exfoliated monolayer films.

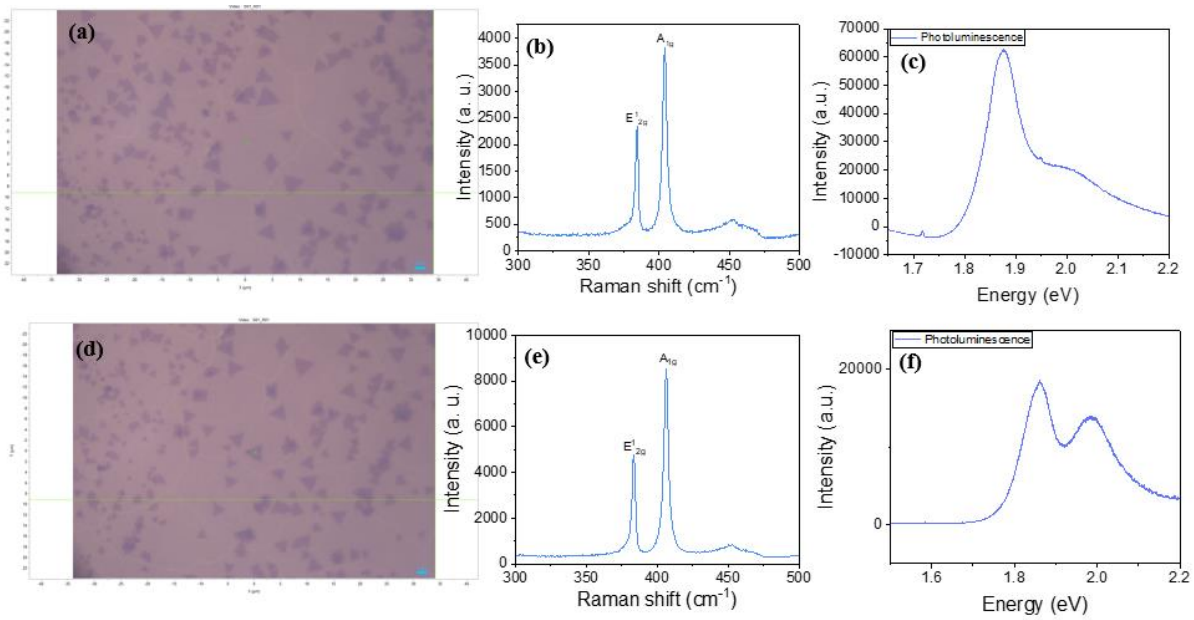

Figure 6: Characterization of MoS_2 grown at 1.5 Torr (a) Optical image (b) Raman spectra of continuous monolayer section (c) PL spectra for continuous monolayer section (d) Optical image of bilayer flake (e) Raman spectra for bilayer flake and (f) PL spectra for bilayer flake

The flakes were also measured and yielded a peak difference of 21.17 cm^{-1} and exciton energy of 1.86 eV, characteristic of bilayer films as shown in Figure 6(d)-(f). This confirms the previous observation for the sample at 1.5 Torr constituting of MoS_2 monolayer with small bilayer flakes.

Figure 7 illustrates the Raman and PL spectra for MoS_2 film grown at 1.75 torr. Measurements on the continuous portion of the film depicts a Raman peak difference of 22.39 cm^{-1} and PL of 1.86 eV. These values agree with exfoliated MoS_2 bilayer and flake

measurements from 1.5 Torr samples. This suggests that increasing pressure permitted greater nucleation and growth of bilayer sites to form a continuous film at 1.75 Torr rather than just isolated flakes. Measurements on isolated adlayer flakes yield a Raman peak difference of 24.17 cm^{-1} and PL of 1.85 eV. These results match those measured from exfoliated MoS_2 tri-layer, confirming nucleation and initial growth of tri-layer on the film.

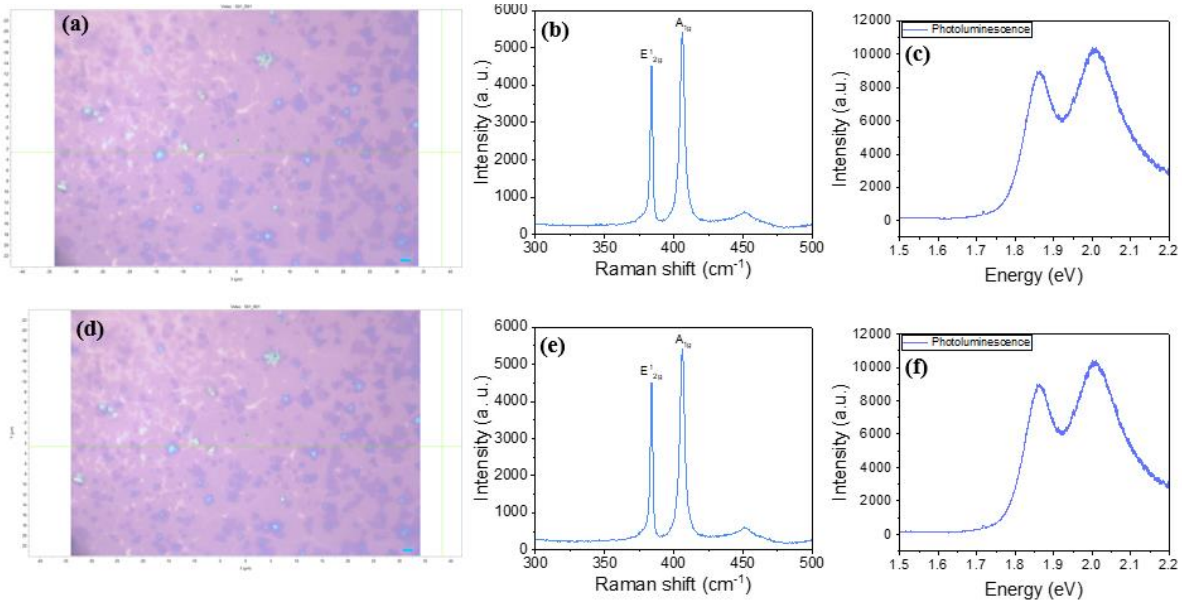

Figure 7: Characterization of MoS_2 grown at 1.75 Torr (a) Optical image (b) Raman spectra of continuous bilayer section (c) PL spectra for continuous bilayer section (d) Optical image of tri-layer flake (e) Raman spectra for tri-layer flake and (f) PL spectra for tri-layer flake

Figure 8 illustrates the Raman and PL spectra for MoS_2 film grown at 2.4 Torr. Measurements yielded nearly identical values to bilayer standards so measurements on the larger flakes were observed instead. These flakes reported a Raman peak difference 25.45 cm^{-1} and PL of 1.82 eV, matching values of exfoliated bulk MoS_2. This supports the trend that increasing flow pressure increases film thickness.

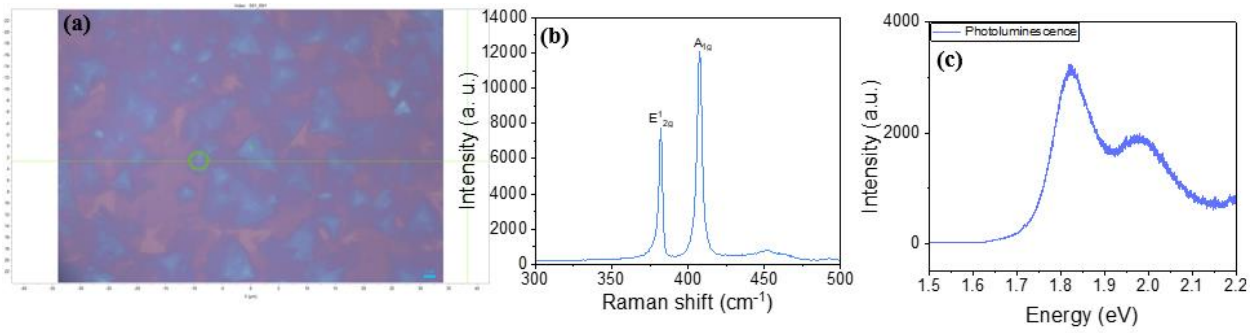

Figure 8: Characterization of MoS_2 grown at 2.4 Torr (a) Optical image (b) Raman spectra of bulk flake section (c) PL spectra for bulk flake

CONCLUSION

To conclude, the effects of the growth parameters time, distance, and flow pressure were investigated to observe their influence on layer thickness, nucleation density, and morphology of MoS_2 films grown by CVD. It was observed increasing flow pressure and growth times increased layer thickness and nucleation density while maintaining morphology. Growth times exceeding 35 minutes were unreliable however due to the increased appearance of surface defects from oxygen chemisorption. Increasing the distance from the precursor was also shown to decrease layer thickness and nucleation density while affecting morphology due to inadequate MoS_2 supply. These trends were confirmed with Raman and PL measurements, suggesting the importance of flow pressure, growth time, relative precursor distance in producing MoS_2 films.

REFERENCES

[1] J. von Neumann, "First draft of a report on the EDVAC," in IEEE Annals of the History of Computing, vol. 15, no. 4, pp. 27-75, 1993, doi: 10.1109/85.238389.

[2] T. Zanotti, F. M. Puglisi and P. Pavan, "Smart Logic-in-Memory Architecture for Low-Power Non-Von Neumann Computing," in *IEEE Journal of the Electron Devices Society*, vol. 8, pp. 757-764, 2020, doi: 10.1109/JEDS.2020.2987402.

[3] Y. Taur, "CMOS design near the limit of scaling," in IBM Journal of Research and Development, vol. 46, no. 2.3, pp. 213-222, March 2002, doi: 10.1147/rd.462.0213.

[4] C. Mead, "Neuromorphic electronic systems," in Proceedings of the IEEE, vol. 78, no. 10, pp. 1629-1636, Oct. 1990, doi: 10.1109/5.58356.

[5] Hodgkin, A.L., Huxley, A.F. A quantitative description of membrane current and its application to conduction and excitation in nerve. Bltn Mathcal Biology 52, 25–71 (1990). https://doi.org/10.1007/BF02459568

[6] Zhao, L., Fan, Z., Cheng, S., Hong, L., Li, Y., Tian, G., Chen, D., Hou, Z., Qin, M., Zeng, M., Lu, X., Zhou, G., Gao, X., Liu, J.-M., An Artificial Optoelectronic Synapse Based on a Photoelectric Memcapacitor. Adv. Electron. Mater. 2020, 6, 1900858.

[7] Sangwan, V.K., Hersam, M.C. Neuromorphic nanoelectronic materials. *Nat. Nanotechnol.* **15,** 517–528 (2020). https://doi.org/10.1038/s41565-020-0647-z

[8] Lee, G., Baek, J.-H., Ren, F., Pearton, S. J., Lee, G.-H., Kim, J., Artificial Neuron and Synapse Devices Based on 2D Materials. Small 2021, 17, 2100640.

[9] Liu, Y., Weiss, N., Duan, X. et al. Van der Waals heterostructures and devices. Nat Rev Mater 1, 16042 (2016). https://doi.org/10.1038/natrevmats.2016.42

[10] Radisavljevic, B., Radenovic, A., Brivio, J. et al. Single-layer MoS2 transistors. Nature Nanotech 6, 147–150 (2011). https://doi.org/10.1038/nnano.2010.279

[11] Fang, M., Wang, F., Han, Y., Feng, Y., Ren, T., Li, Y., Tang, D., Song, Z., Zhang, K., Controlled Growth of Bilayer-MoS2 Films and MoS2-Based Field-Effect Transistor (FET) Performance Optimization *Adv. Electron. Mater.* 2018, 4, 1700524.

[12] Xu, T., Pei, Y., Liu, Y., Wu, D., Shi, Z., Xu, J., Tian, Y., Li, X., High-response NO2 resistive gas sensor based on bilayer MoS2 grown by a new two-step chemical vapor deposition method, Journal of Alloys and Compounds, Vol. 725, 2017, Pages 253-259.

[13] Jeon, J., Jang, S.K., Jeon, S.M., Yoo, G., Jang, Y.H., Park, J.H., and Lee, S., Layer-controlled CVD growth of large-area two-dimensional MoS2 films, Journal of Nanoscale. 2015, Issue 5.

[14] Hussain, S., Shehzad, M.A., Vikraman, D., Iqbal, M.Z., Singh, J., Khan, M.F., Eom, J., Seo, Y., Jung, J., Controlled synthesis and optical properties of polycrystalline molybdenum disulfide atomic layers grown by chemical vapor deposition, Journal of Alloys and Compounds, Volume 653, 2015, Pages 369-378.

[15] Chen, C., Feng, Z., Feng, Y., Yue, Y., Qin, C., Zhang, D., and Feng, W., Large-Scale Synthesis of a Uniform Film of Bilayer MoS2 on Graphene for 2D Heterostructure Phototransistors, ACS Applied Materials & Interfaces 2016 8 (29), 19004-19011

[16] Zhao, S.; Weng, J.; Jin, S.; Lv, Y.; Ji, Z. Chemical Vapor Transport Deposition of Molybdenum Disulfide Layers Using H2O Vapor as the Transport Agent. Coatings 2018, 8, 78. https://doi.org/10.3390/coatings8020078

[17] Yang, Y., Pu, H., Di, J., Zhang, S., Hu, J., Zang, Y., Gao, C., & Chen, C. (2018). Influences of temperature gradient and distance on the morphologies of MOS2 domains. AIP Advances, 8(8), 085218. https://doi.org/10.1063/1.5050652

[18] Liang, T., Xie, S., Huang, Z., Fu, W., Cai, Y., Yang, X., Chen, H., Ma, X., Iwai, H., Fujita, D., Hanagata, N., & Xu, M. (2016). Elucidation of zero-dimensional to two-dimensional growth transition in MOS2chemical vapor deposition synthesis. Advanced Materials Interfaces, 4(4), 1600687. https://doi.org/10.1002/admi.201600687

[19] Yu, Y., Li, C., Liu, Y. et al. Controlled Scalable Synthesis of Uniform, High-Quality Monolayer and Few-layer MoS2 Films. Sci Rep 3, 1866 (2013). https://doi.org/10.1038/srep01866

[20] Chen, F., & Su, W. (2018). The effect of the experimental parameters on the growth of MOS2 flakes. CrystEngComm, 20(33), 4823–4830. https://doi.org/10.1039/c8ce00733k

[21] Marquez, C., Salazar, N., Gity, F., Galdon, J. C., Navarro, C., Duffy, R., Hurley, P., & Gamiz, F. (2021). Performance and reliability in back-gated CVD-grown mos2 devices. Solid-State Electronics, 186, 108173. https://doi.org/10.1016/j.sse.2021.108173

[22] Plechinger, G., Heydrich, S., Eroms, J., Weiss, D., Schüller, C., & Korn, T. (2012). Raman spectroscopy of the interlayer shear mode in few-layer mos2 flakes. Applied Physics Letters, 101(10), 101906. https://doi.org/10.1063/1.4751266

[23] Pierucci, D., Henck, H., Naylor, C. et al. Large area molybdenum disulphide- epitaxial graphene vertical Van der Waals heterostructures. Sci Rep 6, 26656 (2016). https://doi.org/10.1038/srep26656